

pubs.acs.org/acscatalysis Research Article

Identifying Boron Active Sites for the Oxidative Dehydrogenation of Propane

Huan Yan, Selim Alayoglu, Weiqiang Wu, Yongbo Zhang, Eric Weitz, Peter C. Stair,* and Justin M. Notestein*



Cite This: ACS Catal. 2021, 11, 9370-9376



ACCESS

III Metrics & More

Article Recommendations

s Supporting Information

ABSTRACT: Oxidative dehydrogenation of propane (ODHP) to propylene could have a significant impact on the production of this critical chemical intermediate, if appropriate catalysts can be discovered. Recently, heterogeneous catalysts based on boron (oxides and nitrides) have been demonstrated to be promising for ODHP, but their active sites have not been conclusively identified. Here, we report that the deposition of differently sized boronic acids into the micropores of silica



supports results in different distributions of surface borate species after calcination. These materials, in turn, display a wide range of rates in ODHP but similar selectivity, suggesting that they differ only in the numbers of active sites. Features identified by *in situ* Raman, IR, and magic-angle-spinning ¹¹B solid-state NMR spectroscopies are compared to catalyst activity. This correlation identifies the S2 borate species, a hydroxylated nonring boron, as the likely active site and provides a target for directed syntheses of future catalysts.

KEYWORDS: ODHP, NMR, selective oxidation, silica, propylene, precursor

INTRODUCTION

The conversion of light alkanes to partial oxidation products is of great interest to industrial chemistry. Of these, olefins such as propylene are essential raw materials for polymers and fine chemicals.² Propylene is primarily produced by nonoxidative routes because the most commonly reported vanadium oxide catalysts for the oxidative dehydrogenation of propane (ODHP) have only moderate propylene selectivity (\leq 70%) even at low conversion (\sim 15%).³⁻⁶ Recently, boron nitride precatalysts were reported as promising materials for ODHP because of their good selectivity (~75%) at relatively high conversion (\sim 20%). ⁷⁻¹¹ Results have indicated the formation of boron oxide from nitride during the ODHP reaction,9 and the direct use of supported or bulk boron oxides also gave high catalytic performance for ODHP. 12,13 Calculations show that a number of surface borate species are possible under reaction conditions, 14 and there is no consensus on the active site structure on these materials, even from the work on boron oxides for selective oxidation dating back more than 30 years. 15,16 A recent work in ODHP over some boron-based catalysts has included a role for the gas-phase radical species, but the surface initiating species remains unclear. 17,18 Separately, there have been recent studies over boroncontaining zeolites. B-MWW zeolites contain predominantly isolated, in-framework B, and they showed very low ODHP activity. 19 However, in the work published while this article was under review, zeolites containing accessible B-OH sites were shown to be active for ODHP.²⁰ Especially given this latter report, there is a need to further investigate the synthesis and identification of putative active sites for ODHP over supported boron oxides. This will aid computational modeling, confirm the active site assignments in zeolites, and guide the next generation of catalyst design.

Here, we used solution-phase deposition from excess hot toluene/CHCl₃ solutions to graft boronic acids of different sizes onto silica (Figure 1a). Eight precursors were utilized, increasing in size as follows: diboronic acid [B2(OH)4, 1], cyclopropylboronic acid (2), n-hexylboronic acid (3), phenylboronic acid (4), naphthylene-1-boronic acid (5), 9-phenanthracenylboronic acid (6), 4-benzyloxy-1-tert-butoxycarbonylindole-2-boronic acid (7), and FBBBE (C₄₆H₄₆B₂O₉) (8). See Figures S1 and S2 for precursor structures and sizes. Boronic acid derivatives are widely available due to their utility in crosscoupling reactions.²¹ Two silicas were used: one synthesized to have micropores and mesopores (designated as "M" SiO₂) and a commercial silica with only mesopores (designated as "MP" SiO₂). Freshly grafted catalysts with M SiO₂ are denoted as P1-P8, and freshly grafted catalysts with MP SiO₂ are denoted as MP1-MP8 according to the boron precursor used. The materials were then calcined at 600 $^{\circ}\text{C}$ in static air for 4 h to give PX-c and MPX-c, for X = 1-8, where X is the precursor number.

Received: May 13, 2021 Revised: June 22, 2021 Published: July 13, 2021





ACS Catalysis pubs.acs.org/acscatalysis Research Article

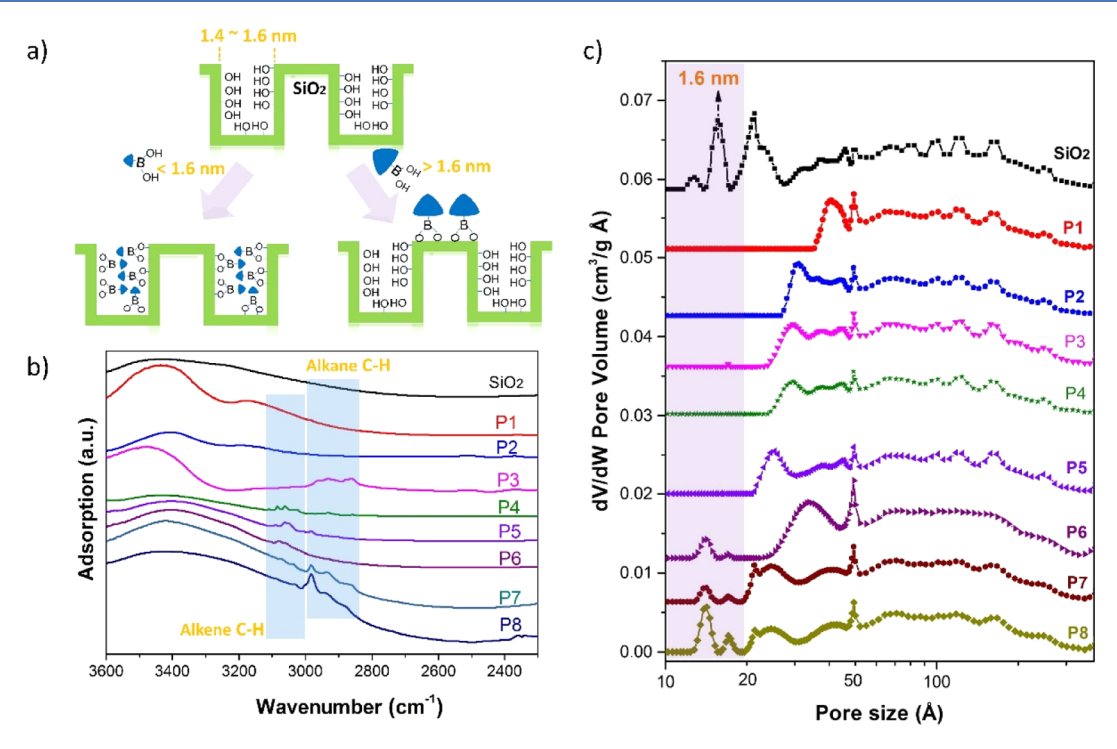


Figure 1. (a) Illustration of the synthesis of silica-supported boron catalysts, (b) DRIFTS spectra of all the as-synthesized boron catalysts, and (c) pore size distributions of the as-synthesized boron catalysts derived from N_2 physisorption isotherms.

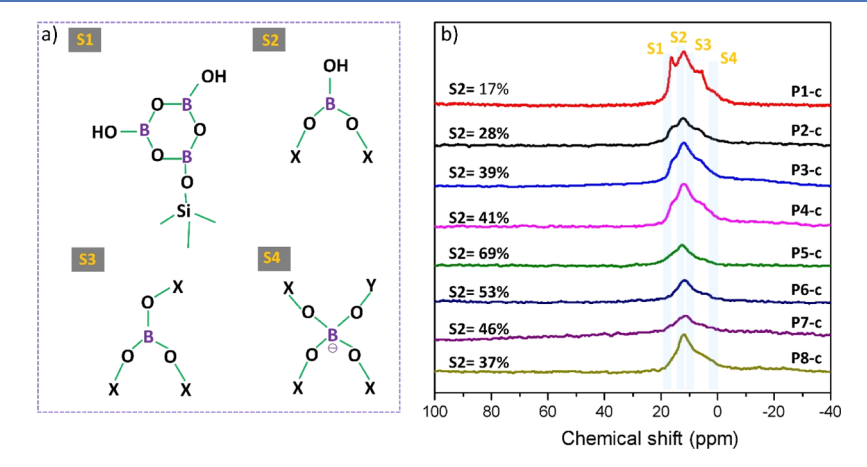


Figure 2. (a) Representation of four potential types of boron species on the SiO_2 surface: S1 is the ring boron; S2 is the hydroxylated nonring boron; S3 is the nonring boron lacking a hydroxyl; and S4 is the tetra-coordinated boron. X = Si or B and Y = Si, B, or H. (b) ^{11}B (MAS) solid-state NMR spectroscopy of all calcined boron catalysts.

■ RESULTS AND DISCUSSION

Boronic acids graft to silica surfaces via surface silanols, ²² as shown by the loss of the Si–OH stretching vibration at 980 cm⁻¹ after deposition (Figure S3). Simultaneously, diffuse reflectance infrared Fourier-transform spectroscopy (DRIFTS) shows the appearance of new vibrations below 3000 cm⁻¹ (alkyl C–H stretches) and above 3000 cm⁻¹ (aromatic C–H stretches) in the freshly grafted materials (Figure 1b). N₂ physisorption shows a clear change in the silica pore size distributions after boronic acid grafting. For materials P1–P5, the original 1.4–1.6 nm micropores disappear after boron grafting (Figures 1c and S4). In contrast, the materials derived from larger precursors, P6–P8, still possessed accessible micropores after grafting. The N₂ physisorption suggests that precursors smaller than ~1 nm freely enter and block the micropores in this material, whereas larger precursors deposit

in the mesopores. Precursor 5 (naphthylboronic acid) is the largest precursor that enters the micropores. Regardless of whether the precursor entered the micropores or mesopores, boron loadings by inductively coupled plasma (ICP) (Figure S5) decreased with the increasing precursor size. For small species such as precursor 2, the boron loading after grafting was 1.5 wt % (surface density of 2.4 B/nm² or 85% of boron in the grafting solution), whereas for larger precursors such as 7 or 8, the boron loading was only 0.2-0.4 wt % (surface density of 0.3-0.4 B/nm²), showing how the deposition location and amount were both limited by the size of the precursor. As seen from B surface densities well below typical silanol densities of 4-5 SiOH/nm², deposition was not limited by available silanols, which persisted after deposition (Figure S3). After calcination in static air at 600 °C, significant physical differences persisted between samples P1-c through P8-c.

ACS Catalysis pubs.acs.org/acscatalysis Research Article

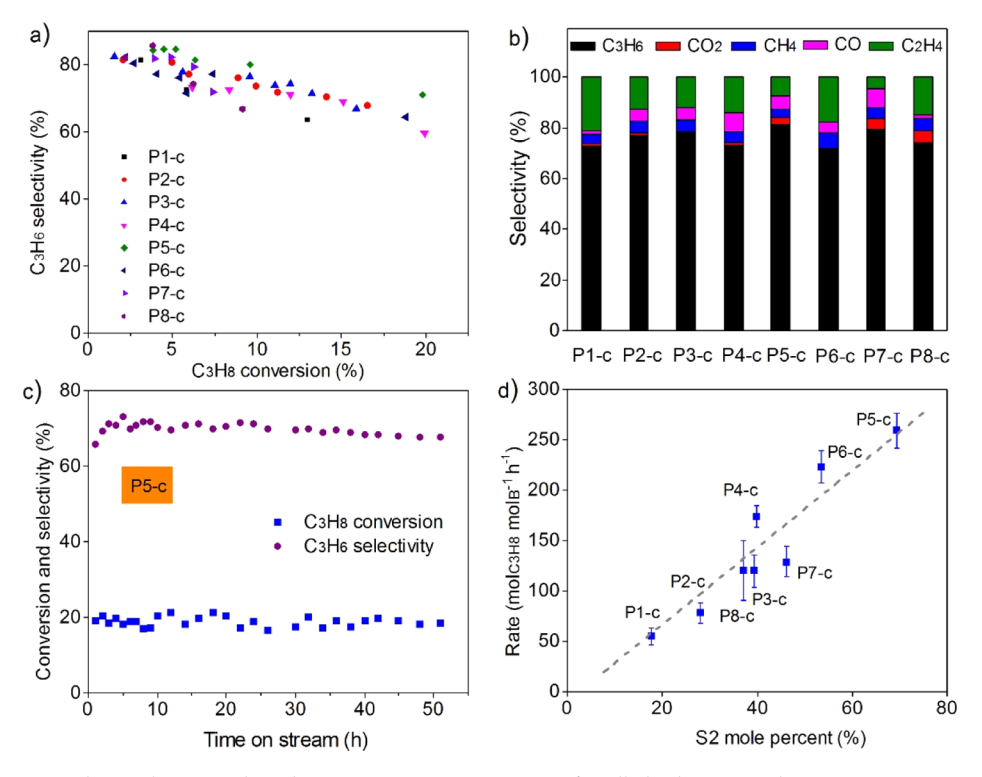


Figure 3. (a) ODHP propylene selectivity plotted against propane conversion for all the boron catalysts. Propane conversion was altered by changing the space velocity. (b) Product distributions for all boron catalysts at a propane conversion of $\sim 6\%$, (c) stability test for the catalyst P5-c, and (d) boron-normalized rate plotted against the mole percent of S2 boron from NMR showing a linear correlation. The percentage of S2 was seen to vary by < 6% absolute depending on the analysis method or prior use in catalysis.

Specifically, P1-c, derived from the smallest precursor, lost all pores below 3.8 nm, materials P2-c through P4-c lost pores below ~2.1–2.5 nm, and materials P5-c through P7-c lost only the smallest pores below 1.8 nm. Finally, P8-c, derived from the largest precursor, had no significant change in porosity relative to the starting silica (Figures S6 and S7).

Next, we used cross-polarized magic-angle-spinning (CP-MAS) ¹¹B solid-state NMR spectroscopy and solid-state line shape analysis to determine if there were differences in boron speciation in addition to the physical differences among the PX-c catalysts. According to the literature, 12,13,23 there are four possible boron species on borosilicate materials: S1 (ring structures), S2 (three-coordinate, nonring B-OH), S3 (threecoordinate, nonring, no B-OH), and S4 (four-coordinate) (Figure 2a). Based on the experimental and calculated ¹¹B NMR spectra (Figures 2b and S8), we deconvoluted the overall spectrum of each material into features from S1 at 18.1 ppm, S2 at 14-15 ppm, S3 at ~11 ppm, 13,19,24,25 and S4 from -0.2 to 1.4 ppm. ^{13, $\overline{23}$,25} We noticed that from P1-c to P5-c, the percent of the total NMR signal that was attributable to S2 increased along with the increase of the precursor size and was the dominant species in the case of P5-c (Figures 2b and S8 and Table S1). For the materials derived from the larger precursors that appeared to not enter the micropores (i.e., P6-c, P7-c, and P8-c), the S2 percentage decreased again. Clearly, bulky precursors confined in micropores favor the formation of the S2 species after calcination. As confirmation, the percentage of S2 changed only slightly for the analysis by direct polarized ¹¹B MAS NMR (39 vs 34% for sample P4-c, Figure S9), and the spectral shapes were not altered by the change in the contact time (1, 2, or 3 ms) in the CP-MAS experiment (Figure S10).

Finally, the calcined boron materials were tested for ODHP. All the catalysts had similar propylene selectivity profiles that decreased with conversion (Figure 3a) and 75-82% propylene selectivity at a fixed 6% conversion (Figure 3b). This selectivity profile is similar to previous reports in the literature discussed above. The catalysts were stable with respect to both catalytic performance and structure; P5-c maintained 72% propylene selectivity at 20% conversion for 50 h without obvious deactivation (Figure 3c), and energy-dispersive X-ray spectroscopy mapping showed that boron was retained after the reaction (Figure S11). The B-OH vibration characteristic of the S2 species persisted after the reaction, as determined by Raman spectroscopy (Figure S12). The CP-MAS ¹¹B NMR of used P5-c (Figure \$13) showed only a small decrease in the percentage of S2 (69-63%) and no large changes to the overall distribution of boron species.

Overall, the catalyst stability and the shared selectivity vs conversion profiles suggest that these materials differ in the total number of active sites but not in the composition of those active sites. Therefore, we compared the B-normalized rates to the S2 percentage discussed above, and it gives a clear linear dependence (Figure 3d). Due to its high S2 percentage, P5-c gave the highest rate of 259 mol_{C3H8} $\text{mol}_{\text{B}}^{-1} \cdot \text{h}^{-1}$. Materials based on larger precursors that could not enter micropores (especially P7-c and P8-c) or those that aggregated due to their small size (especially P1-c and P2-c) gave markedly lower rates. A single turnover frequency (TOF-S2) of $300 \pm 50 \text{ h}^{-1}$ was calculated for all materials based only on the S2 boron species (Figure S14b). Normalizing rates by other boron species (S1, S3, and S4) failed to fit a single value to all boron catalysts in this work, further indicating that the S2 boron

ACS Catalysis pubs.acs.org/acscatalysis Research Article

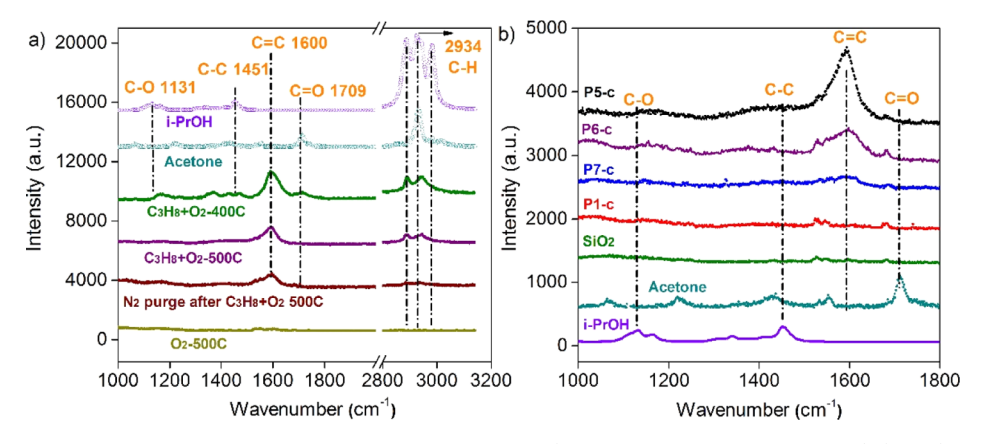


Figure 4. (a) In situ Raman spectra for P5-c catalysts at 400 °C in reaction gas (10% propane, 5% O_2 , balance N_2) (green), 500 °C in reaction gas (purple), and 500 °C in N_2 (dark red) and O_2 (dark yellow), respectively, and (b) in situ Raman spectra at 500 °C in reaction gas for P5-c, P6-c, P7-c, P1-c, and SiO₂. Spectra of acetone and i-PrOH are included as references.

species are likely active sites for the ODHP reaction (Figure S14).

Next, we examined two sets of control materials. To rule out the effect of boron surface density, we synthesized two additional materials: a lower-loaded P2-c and a higher-loaded P7-c, such that they had the same boron surface density as that of P5-c. The B-normalized rates were nearly independent of loading (Figure S15), indicating that the structure of the boron precursor was of overriding importance for the microporous silica support. To examine the effect of support geometry, we examined the catalytic behavior of the boron precursors grafted onto a mesoporous silica support (smallest pores of 2.1-2.5 nm). The freshly grafted materials MP1-MP8 were completely devoid of pores smaller than 3 nm; the smaller mesopores had been filled by the boron precursors, regardless of the precursor size (Figures S16 and S17). Likewise, the ¹¹B NMR S2 percentages were $22 \pm 5\%$ (Figures S18 and S19) for all precursors. After use, the CP-MAS ¹¹B NMR of MP5-c showed only a small increase in the fraction of S2 (23-29%, Figure S13) and no changes to the overall spectral shape. As predicted from the correlation in Figure 3d, the B-normalized rates of the MPX-c catalysts were all similar to each other and lower for nearly all the PX-c catalysts (Figure S20). The S2normalized TOF (TOF-S2) for these materials was 250 ± 50 h⁻¹ (Figure S13b), regardless of the precursor, and only slightly lower than the value obtained over the PX-c catalysts, providing final evidence for S2 as the putative active site. From these control materials, it is clear that micropores are needed to see an effect of the boron precursor size and to maximize the amount of the S2 species. We note that these findings are entirely consistent with recent studies on boron-containing zeolites. A B-MWW material had boron atoms isolated in a silicate framework, but they were only ~10% B-OH S2 sites, resulting in low ODHP reactivity. 19 In contrast, a very recent publication produced active zeolites with highly dispersed boron sites but with a preponderance of B-OH groups nearby Si-OH groups, which formed under reaction conditions.² The work in the current article demonstrates that a preponderance of active sites similar to the above-mentioned sites is also able to be formed inside microporous amorphous silica when a size-matched precursor is used.

We finally used *in situ* Raman spectroscopy to further investigate the structure of the high-performing P5-c catalyst. First, the B-OH feature at 867 cm⁻¹ disappears under reaction conditions, implicating it as an active site (Figure S12).

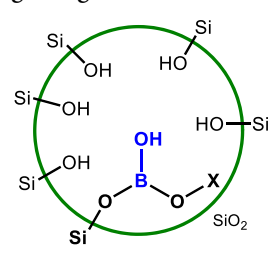
Furthermore, under the atmosphere of 10% propane and 5% O₂ and balance N₂ at 400 °C, a feature appears around 1600 cm⁻¹, which we assign to a C=C vibration, and a pair of features appear around 2934 cm⁻¹, which we assign to C-H vibrations²⁶⁻²⁹ (Figure 4a). Putative C=O (1709 cm⁻¹) and C-O (1131 cm⁻¹) features are assigned with analogy to acetone and isopropanol. The C=O and C-O features disappear when the temperature is raised to the reaction temperature of 500 °C, consistent with the low selectivity to oxygenates or COx over these catalysts. In contrast, the C=Cand C-H features persist at 500 °C and during a N₂ purge at 500 °C but were able to be removed in pure O₂ at 500 °C. One possible assignment for the C=C vibration around 1600 cm⁻¹ would be as conjugated amorphous carbon side products arising from propylene oligomerization, as some of us have previously seen in other weakly acidic systems. 26,28 Alternately. the C=C vibration might arise from surface vinyl or allyl borates 30 that might arise from β -hydride elimination from an alkylborane surface intermediate. For either assignment, this species should grow in proportion to the number of active sites, even if the observed species may not be a reactive intermediate. Consistent with this hypothesis, the in situ Raman spectra of silica (Figures 4b and S21), P1-c (Figures 4b and S22), P6-c (Figure 4b), and P7-c (Figures 4b and S23) showed weaker features near 1600 cm⁻¹. It should be noted that the loading of S2 sites on P1-c is less than that on P5-c, even though P1-c has three times the total boron.

CONCLUSIONS

In summary, we have identified the S2-hydroxylated nonring boron oxide as the putative ODHP active site for silicasupported boron catalysts. Boronic acids of different sizes were deposited on a micropore-containing silica, leading to a variety of surface boron species after calcination. We observed a linear trend between the B-normalized rate and the percentage of S2 boron species detected by NMR, leading to a constant TOF on the basis of S2 boron atoms. This TOF was approximately constant for all eight precursors and slightly dependent on the silica support used. For these materials, a high percentage of S2 appears to arise from a close size match between the support micropores and the precursor; depositing naphthylene-1-boronic acid (precursor 5) on a micropore-containing silica gave \sim 69% S2 boron after calcination and the highest rate per B atom. While 11 B NMR alone cannot distinguish between S2

sites on an isolated B atom and those in a cluster, the low total boron surface densities in these experiments and the recent results in B-containing zeolites suggest that the active species are most likely highly dispersed B-OH species on the silica surface but in close proximity to many SiOH species (Scheme 1). Testing additional borate-treated zeolites³¹ or hydrated

Scheme 1. Proposed S2 Boron Active Site for Propane ODH over Low-Loaded, Microporous Silica Materials, X = Si or B; ¹¹B NMR Alone Cannot Distinguish between S2 Sites on an Isolated B Atom and Those in a Cluster, but the Low Total Boron Surface Densities in These Experiments Suggest That the Active Species Are Most Likely B-OH Species with a High Degree of Isolation



boron-substituted zeolites³² may shed further light on this assignment. Overall, this work identifies a potential active site for ODHP on silica-supported boron catalysts and a template for improving the activity of these materials.

METHODS

Materials. 9-Phenanthracenylboronic acid (95%), 4-benzyloxy-1-tert-butoxycarbonylindole-2-boronic acid, poly(ethylene oxide), and tetraethyl orthosilicate (99%) were purchased from Sigma-Aldrich. Mesoporous SiO₂ (MP, silica gel, high-purity grade, Davisil grade 643, pore volume 1.15 cm³/g) was purchased from Sigma-Aldrich. Tetrahydroxydiboron (95%), cyclopropylboronic acid (97%), n-hexylboronic acid (97%), phenylboronic acid (97%), naphthylene-1-boronic acid (97%), and FBBBE (C₄₆H₄₆B₂O₉) were purchased from Strem Chemicals. Structures and dimensions are shown in Figures

Synthesis of the Silica Support. The "M" SiO₂ support was synthesized *via* the sol-gel process. Typically, 12.5 g of poly (ethylene oxide) was dissolved in 125 g of 1 M HNO₃ at room temperature. Then, 81.25 g of tetraethyl orthosilicate was dropped into the mixture, and the solution was sealed and shaken vigorously until it became homogeneous. The solution was stirred at room temperature for 30 min. Then, the mixture was transferred to an oven at 40 °C and held for 2.5 days. The white gel was cut into small pieces and washed with DI water six times and then washed once with 0.045 M aqueous NH₃. After that, the white gel was heated at 40 °C for 24 h, rinsed with DI water, and heated again at 40 °C for 24 h. Finally, the as-obtained gel was heated at 100 °C for 12 h and then at 600 °C for 12 h in static air.

Synthesis of Boron Catalysts. For the diboronic acid precursor $[B_2(OH)_4$, precursor 1], 1.5 mmol of $B_2(OH)_4$ in 10 mL of DI water and 1 g of freshly synthesized "M" SiO_2 were mixed together, and then, the mixture was dried at 50 °C overnight. For precursors 2–7, 1.63 mmol of organic boron precursor and 1 g of freshly synthesized "M" SiO_2 were mixed together, and then, 35 mL of toluene and 35 mL of chloroform were added into the mixture. Due to the sample limitations of

FBBBE, precursor 8, 0.065 mmol of FBBBE and 200 mg of "M" SiO₂ were mixed together. After sonication for 5 min, the mixture was refluxed at 85 °C for 22 h. After cooling down to room temperature, the as-obtained samples were washed with chloroform five times and dried under dynamic vacuum for 24 h. The as-prepared boron catalysts were designated as P1, P2, P3, P4, P5, P6, P7, and P8 according to the organic boron precursor used. The size of the organic boron precursor used gradually increases from P1 to P8. After calcination at 600 °C under static air for 4 h, the boron catalysts were designated as P1-c, P2-c, P3-c, P4-c, P5-c, P6-c, P7-c, and P8-c, respectively. The synthesis of "MP" SiO₂-supported boron catalysts was carried out following the same process.

To synthesize a material with a higher loading of P7, "M" SiO_2 was pretreated in HCl solution for 2 h at 80 °C, rinsed four times in DI water, and dried at 200 °C in air for 2 h. P7 was then deposited as stated above. To synthesize a material with a lower amount of P2, the amount of P2 in the grafting solution was decreased proportionally.

Catalytic Test. Oxidative dehydrogenation was performed in a nominal atmospheric pressure, quartz tube microreactor. The feed gas consists of 10% propane and 5% oxygen with nitrogen as the balance, and the total flow rate is 16 mL/min. 200 mg of P8-c catalysts and 500 mg of quartz sand were mixed together, and the catalyst was activated at 550 °C for 2 h under feed gas. Then, the reactor was cooled down to 500 °C and we started to collect data. In the case of other boron catalysts, the boron content was kept the same, and the total weight of the catalyst was balanced by pure SiO₂. The different conversions over various boron catalysts at 500 °C were obtained by changing the space velocity. The selectivities and conversions are defined as follows

Conversion =
$$\frac{y_{C_3H_8,0} - y_{C_3H_8}}{y_{C_3H_8,0}} \times 100$$

$$C_{3}H_{6} \text{ selectivity} = \frac{3y_{C_{3}H_{6}}}{3y_{C_{3}H_{6}} + 2y_{C_{2}H_{X}} + y_{CH_{4}} + y_{CO} + y_{CO_{2}}} \times 100\%$$

$$CO_2 \text{ selectivity} = \frac{y_{CO_2}}{3y_{C_3H_6} + 2y_{C_2H_X} + y_{CH_4} + y_{CO} + y_{CO_2}} \times 100\%$$

CO selectivity =
$$\frac{y_{CO}}{3y_{C_3H_6} + 2y_{C_2H_X} + y_{CH_4} + y_{CO} + y_{CO_2}}$$
× 100%

$$CH_{4} \text{ selectivity} = \frac{y_{CH_{4}}}{3y_{C_{3}H_{6}} + 2y_{C_{2}H_{X}} + y_{CH_{4}} + y_{CO} + y_{CO_{2}}} \times 100\%$$

$$C_2 \text{ selectivity} = \frac{2y_{C_2H_X}}{3y_{C_3H_6} + 2y_{C_2H_X} + y_{CH_4} + y_{CO} + y_{CO_2}} \times 100\%$$

$$C_3H_6$$
 yield = $\frac{\text{conversion} \times C_3H_6 \text{ selectivity}}{100}$

where y_i is the mole fraction of product i at the exit of the reactor. The term $y_{\text{C3H8,0}}$ is the mole fraction of propane in the feed gas. Selectivity is on a carbon basis.

Nitrogen Adsorption—Desorption. Nitrogen adsorption—desorption isotherms were measured using a 3Flex (Micromeritics) at -196 °C. Before the measurement, the sample was degassed at 110 °C for 12 h. The specific surface area was calculated from the adsorption data in the relative pressure range from 0.05 to 0.3 using the Brunauer—Emmett—Teller method. Pore size distributions were calculated based on the density functional theory method with a cylinder model.

ICP Optical Emission Spectroscopy. ICP optical emission spectroscopy was performed on a Thermo iCAP 7600 instrument calibrated with boronic acid standards of known concentration. Before the test, all samples were digested in concentrated nitric acid for 6 h at 80 °C.

DRIFTS and *In Situ* Raman Spectroscopy. IR spectroscopy was performed on a Thermo 6700 Fourier-transform infrared instrument. KBr was used as the background in the refection mode. Before performing IR spectroscopy, all materials were heated at 120 °C under air for 2 h. All the IR spectra were collected at room temperature. *In situ* Raman spectroscopy was performed in our custom-built Raman instrument equipped with a 244 nm laser line. The laser power on the sample was about 5 mW, and the data were collected after sample exposure to the laser for 600 s with a 0.155 mm slit. The feed gas consists of 10% propane and 5% oxygen, and the total flow rate is 85 mL/min.

CP-MAS ¹¹B Solid-State NMR Spectroscopy. Solid-state ¹¹B cross-polarized MAS NMR measurements were performed on a three-channel 400 MHz Bruker advance III HD system equipped with both liquid- and solid-state probes. The spectra were acquired using 4 mm MAS NMR probes with a spinning rate of 15 kHz. Samples were loaded into rotors under ambient conditions after calcination at 600 °C under static air for 4 h. The pulse contact time for CP-MAS was varied between 1 and 3 ms and was 2 ms unless stated otherwise. The pulse delay time was 5 s. The 90° pulse was performed for 3.5 μ s at 100 W. The spectra were referenced to Na₂B₄O₇·10H₂O at 2.0 ppm. The spectra were simulated by solid line analysis included in the Bruker Topspin v4.0.7 software. 9,34 The electric field gradient tensor asymmetry parameter, η_0 , was 0 for all species, and the $C_{\rm O}$ (MHz)-quadrupolar coupling constant was 1.6–1.8 for species S1, S2, and S3.

ASSOCIATED CONTENT

Supporting Information

The Supporting Information is available free of charge at https://pubs.acs.org/doi/10.1021/acscatal.1c02168.

¹¹B MAS NMR spectra, adsorption experiments, and *in situ* Raman spectra (PDF)

AUTHOR INFORMATION

Corresponding Authors

Peter C. Stair — Department of Chemistry, Northwestern University, Evanston, Illinois 60208, United States; orcid.org/0000-0001-5654-6000; Email: pstair@northwestern.edu

Justin M. Notestein — Department of Chemical and Biological Engineering, Northwestern University, Evanston, Illinois 60208, United States; ⊙ orcid.org/0000-0003-1780-7356; Email: j-notestein@northwestern.edu

Authors

Huan Yan – Department of Chemistry, Northwestern University, Evanston, Illinois 60208, United States

Selim Alayoglu – Center for Catalysis and Surface Science, Northwestern University, Evanston, Illinois 60208, United States

Weiqiang Wu – Center for Catalysis and Surface Science, Northwestern University, Evanston, Illinois 60208, United States

Yongbo Zhang — Integrated Molecular Structure Education and Research Center, Northwestern University, Evanston, Illinois 60208, United States

Eric Weitz — Department of Chemistry, Northwestern University, Evanston, Illinois 60208, United States; orcid.org/0000-0002-7447-4060

Complete contact information is available at: https://pubs.acs.org/10.1021/acscatal.1c02168

Notes

The authors declare no competing financial interest.

ACKNOWLEDGMENTS

This paper is based upon the work supported primarily by the National Science Foundation under Cooperative Agreement no. EEC-1647722. This work made use of the IMSERC NMR facility at Northwestern University, which has received support from the Soft and Hybrid Nanotechnology Experimental (SHyNE) Resource (NSF ECCS-2025633), Int. Institute of Nanotechnology, and Northwestern University. This work made use of Raman spectroscopy in the REACT facility of the Center for Catalysis and Surface Science (CCSS), which has received support from the Department of Energy (DE-FG02-03ER15457). We acknowledge Professor Marek Pruski (Iowa State University and Ames Laboratory) and Dr. Yuyang Wu (IMSERC) for the discussion of solid-state NMR. All data and images are available in the body of the paper or as the supporting online material.

■ REFERENCES

- (1) Cavani, F.; Teles, J. H. Sustainability in catalytic oxidation: an alternative approach or a structural evolution? *ChemSusChem* **2009**, *2*, 508–534.
- (2) Moulijn, J. A.; Makkee, M.; Van Diepen, A. E. Chemical Process Technology; John Wiley & Sons, 2013.
- (3) Wu, Z.; Kim, H.-S.; Stair, P. C.; Rugmini, S.; Jackson, S. D. On the structure of vanadium oxide supported on aluminas: UV and visible Raman spectroscopy, UV—visible diffuse reflectance spectroscopy, and temperature-programmed reduction studies. *J. Phys. Chem. B* **2005**, *109*, 2793—2800.
- (4) Khodakov, A.; Yang, J.; Su, S.; Iglesia, E.; Bell, A. T. Structure and properties of vanadium oxide-zirconia catalysts for propane oxidative dehydrogenation. *J. Catal.* **1998**, *177*, 343–351.
- (5) Chaar, M. A.; Patel, D.; Kung, H. H. Selective oxidative dehydrogenation of propane over VMgO catalysts. *J. Catal.* **1988**, *109*, 463–467.
- (6) Zhu, H.; Ould-Chikh, S.; Dong, H.; Llorens, I.; Saih, Y.; Anjum, D. H.; Hazemann, J.-L.; Basset, J.-M. VOx/SiO2 Catalyst Prepared by Grafting VOCl3 on Silica for Oxidative Dehydrogenation of Propane. *ChemCatChem* **2015**, *7*, 3332–3339.
- (7) Grant, J. T.; Carrero, C. A.; Goeltl, F.; Venegas, J.; Mueller, P.; Burt, S. P.; Specht, S. E.; McDermott, W. P.; Chieregato, A.; Hermans, I. Selective oxidative dehydrogenation of propane to propene using boron nitride catalysts. *Science* **2016**, 354, 1570–1573.
- (8) Tian, J.; Tan, J.; Xu, M.; Zhang, Z.; Wan, S.; Wang, S.; Lin, J.; Wang, Y. Propane oxidative dehydrogenation over highly selective

- hexagonal boron nitride catalysts: The role of oxidative coupling of methyl. Sci. Adv. 2019, 5, No. eaav8063.
- (9) Love, A. M.; Thomas, B.; Specht, S. E.; Hanrahan, M. P.; Venegas, J. M.; Burt, S. P.; Grant, J. T.; Cendejas, M. C.; McDermott, W. P.; Rossini, A. J.; Hermans, I. Probing the Transformation of Boron Nitride Catalysts under Oxidative Dehydrogenation Conditions. *J. Am. Chem. Soc.* **2018**, *141*, 182–190.
- (10) Grant, J. T.; McDermott, W. P.; Venegas, J. M.; Burt, S. P.; Micka, J.; Phivilay, S. P.; Carrero, C. A.; Hermans, I. Boron and boron-containing catalysts for the oxidative dehydrogenation of propane. *ChemCatChem* **2017**, *9*, 3623–3626.
- (11) Shi, L.; Wang, D.; Song, W.; Shao, D.; Zhang, W.-P.; Lu, A.-H. Edge-hydroxylated Boron Nitride for Oxidative Dehydrogenation of Propane to Propylene. *ChemCatChem* **2017**, *9*, 1788–1793.
- (12) Love, A. M.; Cendejas, M. C.; Thomas, B.; McDermott, W. P.; Uchupalanun, P.; Kruszynski, C.; Burt, S. P.; Agbi, T.; Rossini, A. J.; Hermans, I. Synthesis and Characterization of Silica-Supported Boron Oxide Catalysts for the Oxidative Dehydrogenation of Propane. *J. Phys. Chem. C* 2019, 123, 27000–27011.
- (13) Lu, W.-D.; Wang, D.; Zhao, Z.; Song, W.; Li, W.-C.; Lu, A.-H. Supported Boron Oxide Catalysts for Selective and Low-Temperature Oxidative Dehydrogenation of Propane. *ACS Catal.* **2019**, *9*, 8263–8270.
- (14) Zhang, Z.; Jimenez-Izal, E.; Hermans, I.; Alexandrova, A. N. Dynamic phase diagram of catalytic surface of hexagonal boron nitride under conditions of oxidative dehydrogenation of propane. *J. Phys. Chem. Lett.* **2018**, *10*, 20–25.
- (15) Murakami, Y.; Otsuka, K.; Wada, Y.; Morikawa, A. Partial oxidation of ethane over boron oxide added catalysts. *Chem. Lett.* **1989**, *18*, 535–538.
- (16) Murakami, Y.; Otsuka, K.; Wada, Y.; Morikawa, A. The Partial Oxidation of Ethane over a B2O3-Al2O3 Catalyst. *Bull. Chem. Soc. Jpn.* **1990**, *63*, 340-346.
- (17) Venegas, J. M.; Zhang, Z.; Agbi, T. O.; McDermott, W. P.; Alexandrova, A.; Hermans, I. Why Boron Nitride is such a Selective Catalyst for the Oxidative Dehydrogenation of Propane. *Angew. Chem., Int. Ed.* **2020**, *59*, 16527–16535.
- (18) Zhang, X.; You, R.; Wei, Z.; Jiang, X.; Yang, J.; Pan, Y.; Wu, P.; Jia, Q.; Bao, Z.; Bai, L.; Jin, M.; Sumpter, B.; Fung, V.; Huang, W.; Wu, Z. Radical Chemistry and Reaction Mechanisms of Propane Oxidative Dehydrogenation over Hexagonal Boron Nitride Catalysts. *Angew. Chem., Int. Ed.* **2020**, *59*, 8042–8046.
- (19) Altvater, N. R.; Dorn, R. W.; Cendejas, M. C.; McDermott, W. P.; Thomas, B.; Rossini, A. J.; Hermans, I. B-MWW Zeolite: The Case Against Single-Site Catalysis. *Angew. Chem., Int. Ed.* **2020**, *59*, 6546–6550.
- (20) Zhou, H.; Yi, X.; Hui, Y.; Wang, L.; Chen, W.; Qin, Y.; Wang, M.; Ma, J.; Chu, X.; Wang, Y.; Hong, X.; Chen, Z.; Meng, X.; Wang, H.; Zhu, Q.; Song, L.; Zheng, A.; Xiao, F.-S. Isolated boron in zeolite for oxidative dehydrogenation of propane. *Science* **2021**, 372, 76–80.
- (21) Suzuki, A. Cross-coupling reactions of organoboranes: an easy way to construct C–C bonds (Nobel Lecture). *Angew. Chem., Int. Ed.* **2011**, *50*, 6722–6737.
- (22) Turner, H. M.; Patel, J.; Niljianskul, N.; Chong, J. M. Binaphthol-catalyzed asymmetric conjugate arylboration of enones. *Org. Lett.* **2011**, *13*, 5796–5799.
- (23) Youngman, R. E.; Zwanziger, J. W. Network modification in potassium borate glasses: structural studies with NMR and Raman spectroscopies. *J. Phys. Chem.* **1996**, *100*, 16720–16728.
- (24) Parashar, V. K.; Orhan, J.-B.; Sayah, A.; Cantoni, M.; Gijs, M. A. M. Borosilicate nanoparticles prepared by exothermic phase separation. *Nat. Nanotechnol.* **2008**, *3*, 589.
- (25) Du, L.-S.; Stebbins, J. F. Nature of silicon—boron mixing in sodium borosilicate glasses: a high-resolution 11B and 17O NMR study. *J. Phys. Chem. B* **2003**, *107*, 10063—10076.
- (26) Hackler, R. A.; Kang, G.; Schatz, G. C.; Stair, P. C.; Van Duyne, R. P. Analysis of TiO2 Atomic Layer Deposition Surface Chemistry and Evidence of Propene Oligomerization Using Surface-Enhanced Raman Spectroscopy. *J. Am. Chem. Soc.* **2018**, *141*, 414–422.

- (27) Foti, A.; Barreca, F.; Fazio, E.; D'Andrea, C.; Matteini, P.; Maragò, O. M.; Gucciardi, P. G. Low cost tips for tip-enhanced Raman spectroscopy fabricated by two-step electrochemical etching of 125 μ m diameter gold wires. *Beilstein J. Nanotechnol.* **2018**, 9, 2718–2730
- (28) Masango, S. S.; Hackler, R. A.; Henry, A.-I.; McAnally, M. O.; Schatz, G. C.; Stair, P. C.; Van Duyne, R. P. Probing the chemistry of alumina atomic layer deposition using operando surface-enhanced Raman spectroscopy. *J. Phys. Chem. C* **2016**, *120*, 3822–3833.
- (29) Chua, Y. T.; Stair, P. C. An ultraviolet Raman spectroscopic study of coke formation in methanol to hydrocarbons conversion over zeolite H-MFI. *J. Catal.* **2003**, *213*, 39–46.
- (30) Andrews, L.; Lanzisera, D. V.; Hassanzadeh, P.; Hannachi, Y. Reactions of Laser-Ablated Boron Atoms with Ethylene and Ethane. Infrared Spectra and DFT Calculations for Several Novel BC2H x (x=1, 2, 3, 4, 5) Molecules. *J. Phys. Chem. A* **1998**, *102*, 3259–3267.
- (31) Balyan, S.; Haider, M. A.; Khan, T. S.; Pant, K. Boric acid treated HZSM-5 for improved catalyst activity in non-oxidative methane dehydroaromatization. *Catal. Sci. Technol.* **2020**, *10*, 3857–3867
- (32) Hwang, S.-J.; Chen, C.-Y.; Zones, S. I. Boron sites in borosilicate zeolites at various stages of hydration studied by solid state NMR spectroscopy. *J. Phys. Chem. B* **2004**, *108*, 18535–18546.
- (33) Ding, K.; Gulec, A.; Johnson, A. M.; Drake, T. L.; Wu, W.; Lin, Y.; Weitz, E.; Marks, L. D.; Stair, P. C. Highly efficient activation, regeneration, and active site identification of oxide-based olefin metathesis catalysts. *ACS Catal.* **2016**, *6*, 5740–5746.
- (34) Couto, A. R.; Trovão, C. N.; Rocha, J.; Cavaleiro, A. M. V.; de Jesus, J. D. P. Dalton communication. Solid-state nuclear magnetic resonance studies on the co-ordination geometry of boron in polyoxotungstates. *J. Chem. Soc., Dalton Trans.* 1994, 2585–2586.